

COUPLING ERROR MODEL OF 3-DOF COMPLIANT STAGE BASED ON PARALLELOGRAM MECHANISM

Huaibo Qiang¹), Hongxi Wang¹), Qiang Huang²)

1) Xi'an Technological University, School of Mechatronic Engineering, Xi'an, 710021, China (✉ qianghuaibo@xatu.edu.cn)

2) Northwest Institute of Mechanical & Electrical Engineering, Xianyang, 712099, China

Abstract

Compliant mechanisms are the state-of-the-art in precision Compliant Parallelogram Stage (CPS) due to their many beneficial features. However, the translational motion of CPS is accompanied by parasitic displacement and coupling error in these mechanisms. In this paper, the parasitic displacements are analysed by using the Pseudo-Rigid Body theory on One-Degree of Freedom (1-DoF) CPS firstly. And then the theoretical model of the Coupling Error Transfer Matrix (CETM) is presented on Three-Degree of Freedom (3-DoF) serial CPS. Moreover, the general forms of CETM are developed for the various configurations of 3-DoF compliant mechanisms. In addition, the coupling error model is validated through experiment on 1-DoF CPS. Meanwhile, the analytical results are validated with Finite Element Analysis (FEA) by comparing the parasitic displacements on each coordination axial direction. Compared with the analysis results between theoretical calculation and the FEA method, the maximum difference of the parasitic displacement is about $0.18 \mu\text{m}$ and the relative error of about 6.22%. This result offers the effective ways to calculate and compensate of the coupling errors and serves to facilitate further work regarding the precision analysis of compliant mechanisms.

Keywords: Compliant Parallelogram stage, Parasitic displacement, Coupling error, Transfer matrix.

1. Introduction

Compliant mechanisms constitute a crucial branch of modern mechanics which via the elastic deformation of flexible materials to transmit motion and power [1]. Compared with traditional rigid mechanisms, compliant mechanisms have many advantages as zero backlash, lubrication-free, no friction and wear, smooth and continuous motion, compact structures and displacement resolution up to 1nm [2]. Therefore, they have been extensively employed in high precision applications such as surgical tools, micro-grippers, micro/nano manipulators and even precise measurement mechanism.

Flexure hinges [3], parallel springs [4] and flexible diaphragms [5] are widely used in measurement mechanism and micro-positioning system. For example, the compliant parallelogram plates are employed in both Renishaw SP80 probe and Klingenberg K3D probe [6] that are serve as the translational displacement units. Over the last two decades, compliant mechanism is assuming increasingly critical roles in precise transmission fields. The research activities of compliant mechanism are rapidly increasing due to the extensive applications of Micro-Electro-Mechanical Systems technology.

However, the accompanying parasitic motion and coupling error could adversely affect the displacement accuracy and working characteristics during the process of CPS [7]. Therefore, it is essential to analyse the reason of parasitic displacement and coupling errors on the CPS. These efforts could establish a good foundation for taking reasonable measures to reduce the adverse impact of coupling errors on CPS. So far, some solutions have been proposed to increase the motion precision of compliant mechanism. For instance, the precise movements of

displacement of the flexure hinges were negatively affected by stiffness reduction in bearing directions [8]. Meanwhile, the manufacturing tolerances of flexible beams could adversely affect the bearing direction stiffness and error motions. The theoretical parasitic rotational angle of the compliant module was analysed on account of the axial deformations of the beams [9].

Moreover, the analytical methods have been proposed that were based on the mathematical description of compliant mechanisms. The theoretical models of mechanism natural frequency were established by using the Lagrange Equation [10]. The geometric compatibility equations were combined to describe the coupling effects among kinematic chains [11]. Addressing the issue of parasitic rotation in the compliant mechanisms between the fixed base and motion parts, a non-under-constrained compliant module was developed to constrain the parasitic rotation and lost motion [12]. Furthermore, the analytical method was formulated for parasitic rotation and displacement calculations of CPS [13]. The actuator could obtain continuous linear motion by the parasitic motion of the asymmetrical-trapezoid compliant mechanisms [14].

On the other hand, the several compliant parallelogram units can be assembled in various arrangements. The double parallelogram guide mechanisms were added at the output ends of the bridge-type mechanisms to minimize the parasitic movements of the XY mechanism [15]. The motion errors in the bearing direction could be reduced by arranging two parallelogram compliant modules in a nested parallel arrangement [16]. The existence of complex non-minimum phase zeros was presented in two double parallelogram mechanisms [17]. Additionally, the coupling motion of compliant parallelogram modules would be partially eliminated because the topology structure was kineto-statically decoupled [18].

Based on previous studies, the current research on parasitic displacement and error compensation has been mostly limited in single degree of freedom mechanisms. Meanwhile, it is largely focused on theoretical model of flexible elements and analysis of the relationship between load and stiffness. Yet little research has been done on the coupling error of multi-degrees of freedom CPS comparatively.

This paper presents a novel theoretical model on parasitic displacement and coupling error which are the research highlights on the CPS. A series of 3-DoF CPS is proposed in Section 2. The CETM of the 3-DoF CPS is established and the coupling errors relationships are described under different topological structures in Section 3. The correctness of this theoretical model is verified by the experiment investigation and FEA simulation. Finally, Conclusions are given in Section 5.

2. The principle of 3-DoF translational stage

The common compliant structural forms include flexure hinge, flexible beam [2], parallel spring [4] and flexible diaphragms [6]. In the field of MEMS systems, flexible elements are used as translational or guiding mechanism with the displacement reaching the micro-meter level. They are often composed of single parallelogram unit or several parallelogram units to meet high-precision and large-stroke transmission requirements. Fig. 1 shows the schematic diagram of a series model of 3-DoF translational mechanism. The centre of measuring ball is defined as the coordinate origin O while the directions of the three orthogonal axes are the x axis, y axis and z axis respectively. The reverse direction of the stylus feed is defined as the z axis. The complex spatial movements could be decomposed and guided by means of the translational motion on each axial compliant guidance units.

The displacements of each translational unit are measured through the internal sensors of the compliant mechanisms. Hence, the geometric information will be calculated according to the measurement point information such as the size and shape of the measured objects. The input driving force is transmitted to the compliant guidance mechanism by the stylus when the external measuring stylus contacts the measured object. The general working stroke range of a

precision 3D scanning probe is $\pm 1\sim 2.5$ μm , the measurement driving force is $\pm 0.1\sim 0.5$ N and the resolution can reach the level as $0.01\sim 0.02$ μm [19].

The sliding or rolling guide pairs were rarely used in the guiding mechanism of precision translational motion because these guide pairs are not only depended on the relative contact surface to provide certain preloading force and reasonable lubrication conditions, but also depended on some reset devices to ensure the smoothness and continuity of guiding movement.

However, these pairs are difficult to meet the performance requirements of the guiding mechanism in precise measurement or positioning systems. Ideally, the transmission process of translational mechanism is approach to frictionless, gapless and compact. These approaches make it easy to use Compliant Parallelogram stage to construct miniaturized or even miniaturized translational motion mechanisms. Hence, it is suitable as a CPS for precise positioning or micro-measurement systems [20].

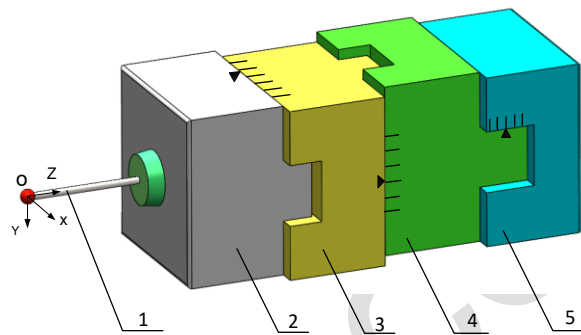


Fig. 1. The series model of 3-DoF translational stage, 1) stylus, 2) the x -axial translational unit, 3) the y -axial translational unit, 4) the z -axial translational unit, 5) the fixed base.

3. Coupling error of CPS

The parasitic displacement is an accompanying displacement which is generate in the vertical direction of the main motion direction in mechanisms. The coupling effect among different motion units would have significant influence on the motion accuracy and performance of the integral CPS.

For example, the 3-DoF compliant translational units of a precision scanning probe can be combined in series, parallel or series parallel hybrid structure. The coupling errors and parasitic displacements are presented different forms according to these various topological structures. Therefore, it is necessary to analyse the principle of coupling errors on different configuration of CPS. And some reasonable measures could be taken for reducing the negative impact of coupling errors on CPS.

3.1. Parasitic displacement of 1-DoF CPS

Figure 2 shows the pseudo-rigid-body model of 1-DoF Compliant Parallelogram Stage. Therein the undeformed initial situation is represented by solid lines and the deformed situation is represented by dashed lines. According to the pseudo-rigid body theory [21, 22], the flexible guide plate is equivalent to a rigid element and the flexure hinges at both ends for each guide plate which are equivalent to the ideal rotational pairs. This CPS is fixed to the base and loaded with the input driving force F on the end of the stylus. The pseudo-rigid-body angle θ of the compliant guide plates is caused by the elastic deformation of the flexure hinges. The parasitic

displacement δ in the y-axis direction is caused by the translational displacement Δx in the x-axis direction which can be represented as:

$$\delta = l - \sqrt{l^2 - \Delta x^2} \quad (1)$$

where l is the length of the compliant guide plates. The dimensionless expression λ is introduced which is defined as $\lambda = \Delta x / l$. The parameter η can be expressed as $\eta = \delta / l$ in the coupling error coefficient of the CPS, then the (1) can be written as:

$$\eta = 1 - \sqrt{1 - \lambda^2} \quad (2)$$

The translational displacement Δx is along the main motion direction by the input driving force F while the direction vector of parasitic displacement δ is perpendicular to the translational displacement Δx . Furthermore, the parasitic displacement δ is affected on the material and some structural parameters of the two compliant plates. Generally, there is $\Delta x \leq l$ in the precision translational guidance and micro-positioning mechanisms.

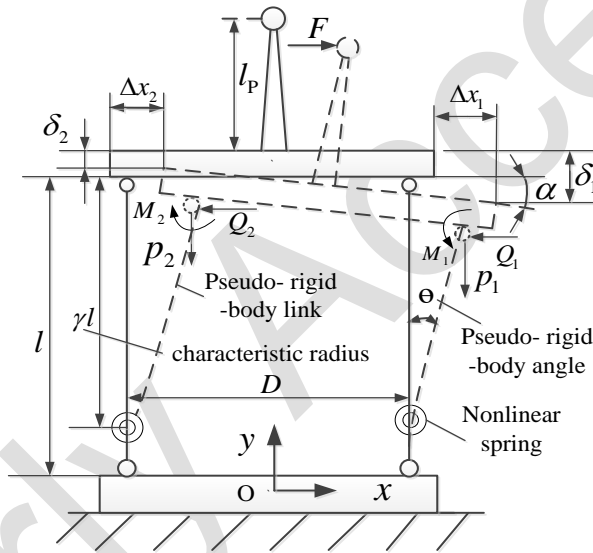


Fig. 2. The pseudo-rigid-body model of 1-DOF CPS.

If the polynomial $\sqrt{1 - \lambda^2}$ is expanded by using the Taylor expansion:

$$\sqrt{1 - \lambda^2} = 1 - \frac{\lambda^2}{2} + \dots + R_n(\lambda) \approx 1 - \frac{\lambda^2}{2} \quad (3)$$

If the formula (3) is substituted into the (2), the error coupling coefficient is obtained as:

$$\eta = \frac{1}{2} \lambda^2 = \frac{1}{2} \left(\frac{\Delta x}{l} \right)^2 \approx \frac{1}{2} \theta^2 \quad (4)$$

In (4), the driving force F is the combined acting on the compliant guide plates on both sides of parallelogram mechanism. The value of pseudo-rigid-body angle θ is the ratio of the translational displacement Δx to the length l of complaint plates. According to the equation in the references [23], the parasitic displacement δ can be expressed as:

$$\delta = l - \gamma l \sin \theta = l(1 - \gamma \sin \theta) \quad (5)$$

Here, γ is the characteristic radius factor. A simple rule-of-thumb for γ in rough calculations is $\gamma = 0.85$. Once γ is determined, the deflection path may be parameterized in terms of θ , the pseudo-rigid-body angle. For this reason, the pseudo-rigid-body angle θ will increase accordingly when the CPS is improved to achieve a large stroke, but the parasitic displacement δ will be decreased conversely. As a result, the larger value of the pseudo-rigid-body angle θ would not affect the estimation of parasitic displacements in compliant guiding mechanisms.

The parasitic rotation of the guiding plate is caused when the axial deformations of the two compliant plates are considered. With a right horizontal force F acting on the translational plate, the left compliant plate will be extended by an axial force P_2 and the right compliant plate will be compressed by another axial force P_1 . The parasitic displacement δ_1 and δ_2 are the axial deformation of the right and the left compliant plate respectively. The parameter α is the parasitic angle of the guiding plate and D is the distance between two compliant plates. As the symmetry of this structure about y-axis, the force F and moment M acting on two compliant plates are almost the same. From the geometry relations and balance of forces and moment in Fig. 2, the following equations can be presented as:

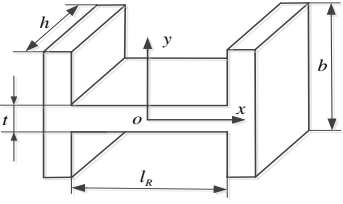
$$\begin{cases} M_1 + M_2 - Fl_p \cos \alpha + (Q_1 + Q_2) \frac{D}{2} \sin \alpha + (P_1 + P_2) \frac{D}{2} \cos \alpha = 0 \\ D \sin \alpha + \delta_2 = \delta_1 \\ \Delta x_1 = \Delta x_2 = -\frac{Q_1 l^3}{3EI} = -\frac{Q_2 l^3}{3EI} \\ F = P_1 + P_2 \end{cases} \quad (6)$$

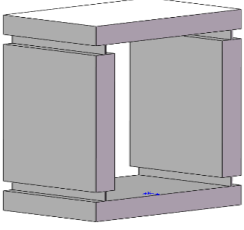
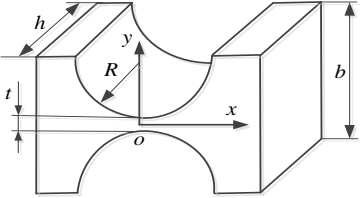
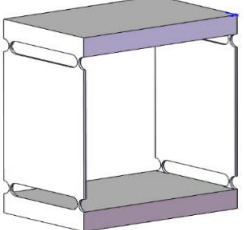
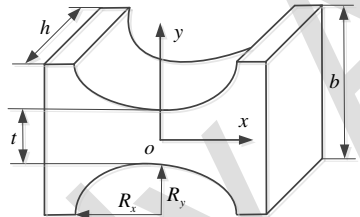
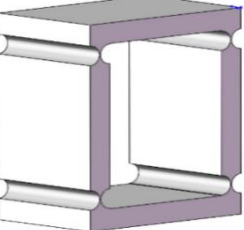
Where, α is very small angle in small deformation, then $\sin \alpha \approx \alpha$ and $\cos \alpha \approx 1$, so the parasitic angle of this CPS can be calculated as below:

$$\alpha = \frac{F(l + l_p)^2}{E(hlD^2 + 4I)} \quad (7)$$

This type of 1-DoF CPS is applied in the precision mechanisms such as the scanning probe or precise positioning mechanism. And the range of displacement is several milli-meters and the driving force F is relatively smaller, for instance, it is commonly little as 0.5N approximately. When the length of stylus is $l_p = 28\text{mm}$ and the values of other parameters is shown in following Tab.2, The calculated value of parasitic angle α is $2.08 \times 10^{-7}^\circ$. Therefore, the parasitic motion of the guiding plate can be negligible.

Table 1. The stiffness of three type compliant stages with their corresponding flexure hinges.

Types	The structure of complaint units	The formula of stiffness
Rectangular Flexure Hinge		$K_{hinge} = \frac{Eht^3}{12l_R}$

<p>The CPS is built with rectangular flexure hinges</p>		$K_{stage} = \frac{Eht^3}{3l_R l^2}$
<p>Right-circular Flexure Hinge</p>		$K_{hinge} = \frac{Eh^3}{24 \left(\frac{t+2R}{\sqrt{t(t+4R)}} \arctan \left(\frac{t+2R}{\sqrt{t(t+4R)}} \right) - \frac{\pi}{4} \right)}$
<p>The CPS is built with right-circular flexure hinges</p>		$K_{stage} = \frac{Eh^3}{6l^2 \left(\frac{t+2R}{\sqrt{t(t+4R)}} \arctan \left(\frac{t+2R}{\sqrt{t(t+4R)}} \right) - \frac{\pi}{4} \right)}$
<p>Elliptical Flexure Hing</p>		$K_{hinge} = \frac{Eha_y^3}{12a_x} \left[\frac{12(a_y/t)^4 (2a_y/t+1)}{(4a_y/t+1)^{5/2}} \arctan \sqrt{4a_y/t+1} + \frac{2(a_y/t)^3 \left(\frac{16a_y^2}{t} + 4a_y/t+1 \right)}{(4a_y/t+1)^2 + 2(a_y/t+1)} \right]^{-1}$
<p>The CPS is built with elliptical flexure hinges</p>		$K_{stage} = \frac{Eha_y^3}{3a_x l^2} \left[\frac{12(a_y/t)^4 (2a_y/t+1)}{(4a_y/t+1)^{5/2}} \arctan \sqrt{4a_y/t+1} + \frac{2(a_y/t)^3 \left(\frac{16a_y^2}{t} + 4a_y/t+1 \right)}{(4a_y/t+1)^2 + 2(a_y/t+1)} \right]^{-1}$

The different flexure hinges are adopted in various compliant mechanisms, such as rectangular flexure hinge, right-circular flexure hinge and elliptical flexure hinges. The similar structure of 1-DoF CPS is built with different flexure elements. The distinct stiffness of these flexure hinges and the stiffness of 1-DoF CPS are listed in Table.1 respectively.

The parameters t is the minimum thickness which is an important indexes of stiffness performance in flexure hinge. The stiffness K_{hinge} of flexure hinge would increase with the increase of the minimum thickness t .

Based on the theory of Flexible Beam Bending principle, the swing angle of the single-sided compliant guide plates is $\theta = Fl^2 / 4EI$. The elastic modulus E should be corrected to the plane

elastic modulus E' when the ratio of width b to thickness h is more than 10 times about the compliant guide plates. And the correction relationship is shown in (8):

$$E' = \frac{E}{1 - \mu^2} \quad (8)$$

In the above equation, the parameter μ is the Poisson's ratio flexible material of the compliant guiding plates. The parasitic displacement δ of 1-DoF on CPS can be expressed as:

$$\delta = \frac{F^2 l^5}{32(E'I)^2} \quad (9)$$

Where $E'I$ are the bending stiffness and the section is a rectangular of the compliant guide plates. The moment of inertia is $I = lh^3/12$ when the bending deformation occurs in the compliant plates. Therefore, in such case, the expression of the parasitic displacement δ is adapted as:

$$\delta = \frac{9F^2 l^5}{2E'^2 h^6} \quad (10)$$

3.2. Coupling error of 3-DoF CPS

The more of degree of freedom in compliant mechanisms, the more parasitic displacement and coupling error would be exist in these mechanisms. The coupling errors are an important source of errors in compliant mechanism such as precision probes, micro positioning system. This research focuses on exploring the principles of coupling error in compliant stage and establishing the *Coupling Error Transfer Matrix* (CETM). The endeavour aims are to develop the theoretical model for improving the motion accuracy and comprehensive performance of CPS. In this section, three units of 1-DoF CPS have been arranged in series to constitute a 3-DoF compliant guiding mechanism in probe, as shown in Fig. 3. The axial direction of the stylus is defined as z -axis. Some insignificant factors have been disregarded such as deformation of the stylus and radius errors of the measuring ball in this paper.

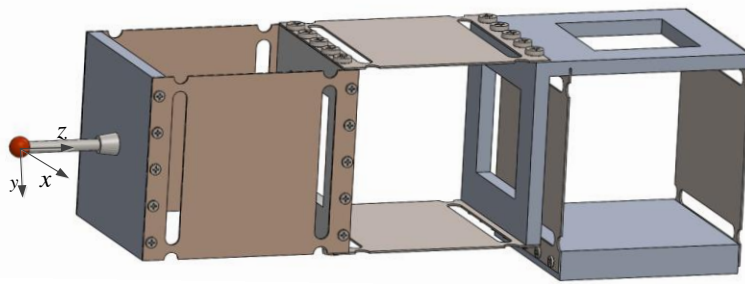


Fig. 3. A series configuration of 3-DoF CPS.

Assuming the ideal translational output displacements are $\Phi = (\Delta x, \Delta y, \Delta z)^T$ by three sensor units that are equipped inside each compliant stage.

According to the achievements above, it can be concluded that there are coupling errors in the compliant guidance mechanism along the three coordinate axes. The CETM of the 3-DoF compliant parallelogram guidance mechanism is expressed as:

$$\Gamma = (\delta_{ij}) \quad (11)$$

In this equation, the δ_{ij} represents the coupling error of compliant stage in i -axial direction, which is caused by the motion of the compliant stage in j -axial direction, where $i, j = x, y, z$. The actual output translational displacement of the 3-DoF compliant translational mechanism can be defined as $\Lambda = (x_p, y_p, z_p)^T$:

$$\Lambda = \Phi + \Gamma \quad (12)$$

$$\begin{bmatrix} x_p \\ y_p \\ z_p \end{bmatrix} = \begin{bmatrix} \Delta x \\ \Delta y \\ \Delta z \end{bmatrix} + \begin{bmatrix} \delta_{xx} & \delta_{xy} & \delta_{xz} \\ \delta_{yx} & \delta_{yy} & \delta_{yz} \\ \delta_{zx} & \delta_{zy} & \delta_{zz} \end{bmatrix} \begin{bmatrix} 1 \\ 1 \\ 1 \end{bmatrix} = \Phi + \delta_{ij} e^r \quad (13)$$

where δ_{xx} , δ_{yy} , δ_{zz} are the inherent characteristic errors of the internal sensors of the CPS. Assuming that the inessential influence of inherent characteristics of each sensor has been ignored in the complaint mechanism, so there is $\delta_{xx} = \delta_{yy} = \delta_{zz} = 0$, the (13) can be written as:

$$\begin{bmatrix} x_p \\ y_p \\ z_p \end{bmatrix} = \begin{bmatrix} \Delta x \\ \Delta y \\ \Delta z \end{bmatrix} + \begin{bmatrix} 0 & \delta_{xy} & \delta_{xz} \\ \delta_{yx} & 0 & \delta_{yz} \\ \delta_{zx} & \delta_{zy} & 0 \end{bmatrix} \begin{bmatrix} 1 \\ 1 \\ 1 \end{bmatrix} = \Phi + \Gamma e^r \quad (14)$$

Considering the configuration relationship of the 3-DoF compliant guidance mechanism in Fig. 3. The three axial translational displacement is measured respectively by each sensor which is installed inside each stage. Owing to the parasitic displacements of the y-axial and z-axial CPS present without along the x-axis. The result of the x-axial sensor only contains the translational displacement of the x-axial CPS, resulting in $\delta_{xy} = 0, \delta_{xz} = 0$.

Meanwhile, the coupling impact of the z-axial CPS will not act on the y-axial CPS because the parasitic displacement of the z-axial CPS presents along y-axis while parasitic displacement of the x-axial CPS is not act along the y-axial CPS, so $\delta_{yx} = 0, \delta_{yz} = 0$.

For the same reason, the parasitic displacements of the x-axial and y-axial CPS both present along the z-axis, thus the result of the z-axial sensor not only comprise the translational displacement of the z-axial CPS, but also comprise the parasitic displacements of the x-axial and y-axial CPS simultaneously. Therefore, the corresponding matrix elements should be considered as $\delta_{zx} \neq 0, \delta_{zy} \neq 0$.

Therefore, the relationship expression can be obtained between the actual output translational displacement $(x_p, y_p, z_p)^T$ and the measurement results $(\Delta x, \Delta y, \Delta z)^T$ along with three axes of the compliant mechanism as follows:

$$\begin{cases} x_p = \Delta x \\ y_p = \Delta y + \delta_{yz} \\ z_p = \Delta z + \delta_{zx} + \delta_{zy} \end{cases} \quad (15)$$

Then the CETM Γ of this compliant parallelogram mechanism can be expressed as:

$$\Gamma = \begin{bmatrix} 0 & 0 & 0 \\ 0 & 0 & \delta_{yz} \\ \delta_{zx} & \delta_{zy} & 0 \end{bmatrix} \quad (16)$$

Based on the research conclusion of parasitic displacement model of 1-DoF CPS above, the stroke ratio is $\lambda_i = \Delta i / l_i$ ($i = x, y, z$). According to the formulas (1) and (9), the coupling error on the z -axial complaint stage which is caused by the motion of the x -axis directional CPS can be calculated as:

$$\delta_{zx} = (1 - \sqrt{1 - \lambda_x^2}) l_x = \frac{F_x^2 l_x^5}{32(E'I)^2} \quad (17)$$

For the same reason, the coupling error on the z -axial complaint stage caused by the motion of the y -axis directional complaint parallelogram stage can be stated as:

$$\delta_{zy} = (1 - \sqrt{1 - \lambda_y^2}) l_y = \frac{F_y^2 l_y^5}{32(E'I)^2} \quad (18)$$

Similarly, the coupling error on the y -axial complaint stage caused by the motion of the z -axis directional complaint parallelogram stage can be stated as:

$$\delta_{yz} = (1 - \sqrt{1 - \lambda_z^2}) l_z = \frac{F_z^2 l_z^5}{32(E'I)^2} \quad (19)$$

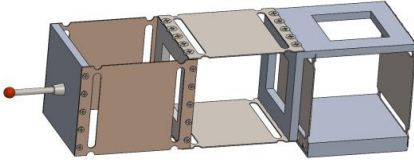
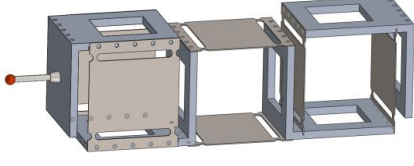
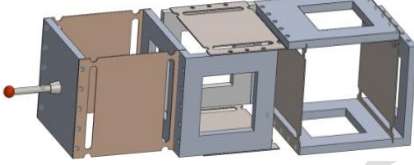
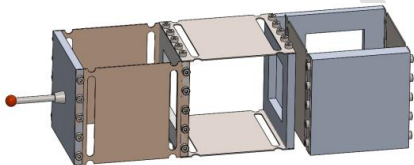
In the formula, F_x , F_y and F_z are the components of the input driving force in the three coordinate axes respectively. The cross-sectional shape of the compliant guide plates is rectangular. Assuming the characteristics of the compliant guide plates are consistent in same terms of materials, structure and cross-sectional dimensions. The matrix of the CETM Γ is then expressed as the following formula(20).

From the (14), it can be observed that the element of the CETM Γ would various because of the different forms of 3-DoF CPS. By substituting the above results into the (12), the output translational displacement can be obtained which contains the coupling errors $\Lambda = (x_p, y_p, z_p)$ of the 3-DoF CPS.

$$\Gamma = \frac{1}{64} \begin{bmatrix} 0 & 0 & 0 \\ 0 & 0 & \frac{F_z^2 l_z^5}{(E'I)^2} \\ \frac{F_x^2 l_x^5}{(E'I)^2} & \frac{F_y^2 l_y^5}{(E'I)^2} & 0 \end{bmatrix} \quad (20)$$

The different topological configurations of CETM can be developed if the spatial position and connection form of several compliant mechanism are altered in Fig. 3. The form of CETM is independent of the combination order of the 3-DoF CPS. Nevertheless, the form of CETM is related to the coordinate axial vectors of each compliant mechanism. The position of elements in the CETM would change only if some compliant mechanism has rotated $\pm \pi/2$ phase angle about its own axis. The normal form of the CETM of the 3-DoF CPS is listed in Table 2.

Table 2. The forms of CETM according to the different configuration of 3-DoF CPS.

Assembly scheme	The configuration of CPS	The form of CETM
$x \rightarrow y \rightarrow z$		$\begin{bmatrix} 0 & 0 & 0 \\ 0 & 0 & \delta_{yz} \\ \delta_{zx} & \delta_{zy} & 0 \end{bmatrix}$
x -axial CPS rotates $\frac{\pi}{2}$ $\rightarrow y \rightarrow z$		$\begin{bmatrix} 0 & 0 & 0 \\ \delta_{yx} & 0 & 0 \\ \delta_{zx} & \delta_{zy} & 0 \end{bmatrix}$
$x \rightarrow$ y -axial CPS rotates $\frac{\pi}{2}$ $\rightarrow z$		$\begin{bmatrix} 0 & \delta_{xy} & 0 \\ 0 & 0 & 0 \\ \delta_{zx} & \delta_{zy} & 0 \end{bmatrix}$
$x \rightarrow y \rightarrow$ z -axial CPS rotates $\frac{\pi}{2}$		$\begin{bmatrix} 0 & 0 & \delta_{xz} \\ 0 & 0 & 0 \\ \delta_{zx} & \delta_{zy} & 0 \end{bmatrix}$

For multi-DoF CPS with parallel relationship, the connection and coupling relationship should be analysed firstly, the CETM as the (14) can be established according to the combination form of CPS.

For instance, as in Fig. 3, the CETM will remain the 3×3 matrix while the y -axial CPS is parallel to the x -axial CPS. Then the coupling impact of the y -axial CPM on the z -axial CPS is the same as that is effect on the x -axial CPM, so $\delta_{zy} = 0$ and $\delta_{zx} = 0$. Similarly, there are $\delta_{zx} \neq 0$ and $\delta_{zy} \neq 0$ when the x -axial CPM is parallel to the y -axial CPS in 3-DoF CPS.

4. FEM and experimental investigation

The prototype of the 1-DoF CPS was fabricated and evaluated with varying experimental parameters. Furthermore, the validation of analytical results on coupling error model was provided by FEA-simulation in commercial software ANSYS Workbench software.

4.1. Analysis on 1-DoF CPS

The right-circular flexure hinge was constructed with the performance parameters and dimensions listed in Table 3. The compliant guide plates were fabricated by the wire-electrode cutting technique which offers a manufacturing tolerance of $\pm 2 \mu\text{m}$. The other components of the assembly were fabricated by traditional machining including the translational plates and fixed base.

Table 3. The parameters of flexure hinge and compliant plate.

Parameter name	Symbol	Value	Unit
Elastic Modulus of flexure element	E	1.95×10^{11}	GPa
the Poisson's ratio of flexure element	μ	0.30	
The length of compliant plate	l	50.00	mm
The thickness of compliant plate	h	0.30	mm
The radius of flexure hinges	R	1.50	mm
The thickness of compliant plate	t	1.00	mm
The distance between two compliant plates	D	50	mm

The material of the compliant guide plates was selected as stainless steels with Young's modulus of $E = 195$ GPa. Meanwhile, the material of the translational plate and the fixed plate was selected as Aluminium alloy with the Young's modulus of $E = 73$ GPa, respectively. Besides the stylus, the whole size (Length \times Width \times Height) of 1-DoF compliant mechanism is $50 \text{ mm} \times 50 \text{ mm} \times 55 \text{ mm}$.

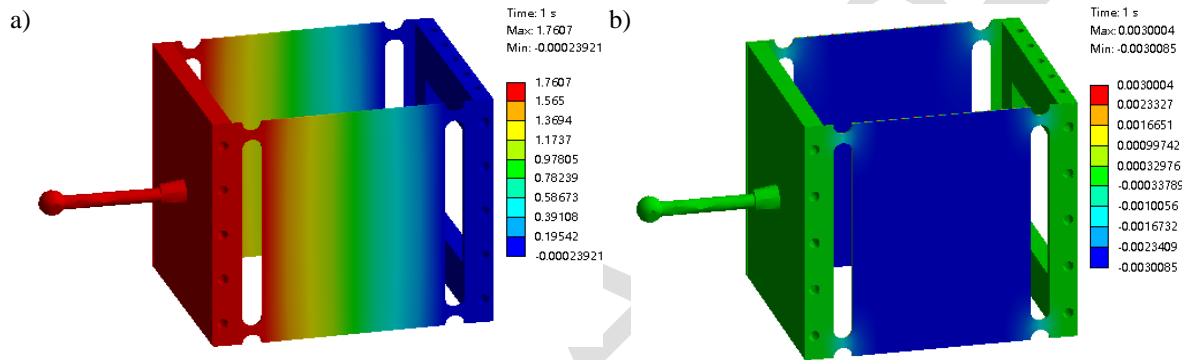


Fig. 4. Finite element results on 1-DoF CPS

(a) The translational displacements in x -axis, (b) The parasitic displacements in z -axis.

As shown in Fig. 4, the fixed constraints were applied on above and below of the mounting base. Since the stiffness of the translational plates and mounting base is much higher than that of the compliant guide plates, all of the translational plates and mounting base including the stylus were set to have the behaviour as rigid stiffness.

The size for flexure hinges was set as 0.01 mm on the local element mesh. The input driving force was added matching the overall stiffness of this compliant mechanism that the range of the force is 0~1 N and the step-size was 0.1 N.

According to the FEA simulation, the maximum translational displacement in x -axis is 1.7607 mm and the maximum parasitic displacements is 0.003 mm over the full travel range of the external driving force, respectively.

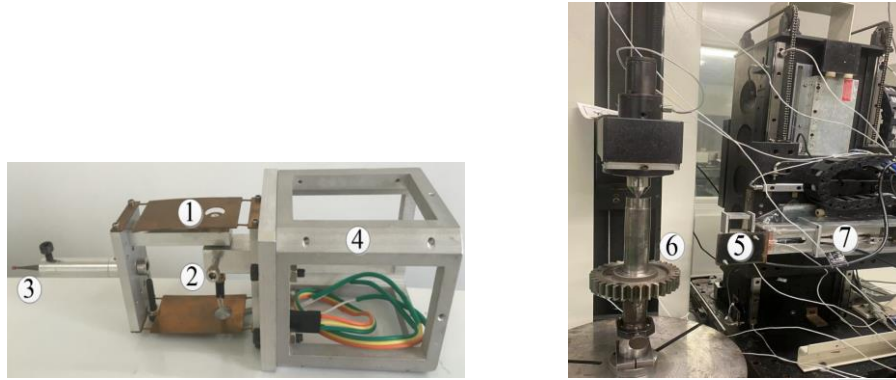


Fig. 5. Experimental setup with its components 1) CPS, 2) sensor, 3) stylus, 4) mounting base, 5) 1-DoF CPS, 6) tested object, 7) driving mechanism.

For the verification of the FEA results, the experimental setup was developed as shown in Fig. 5. The 1-DoF compliant guiding mechanism was installed on the CNC gear measurement device. The servo driving unit of this experimental setup was adopted by high precision rolling screw-nut mechanism. Two-channel displacement information were identified effectively by LVDT differential displacement sensors.

Based on this experimental data, the theoretical curve, FEA results and experimental curve of the translational displacement and the parasitical displacement on the CPS were drawn as shown in Fig. 6.

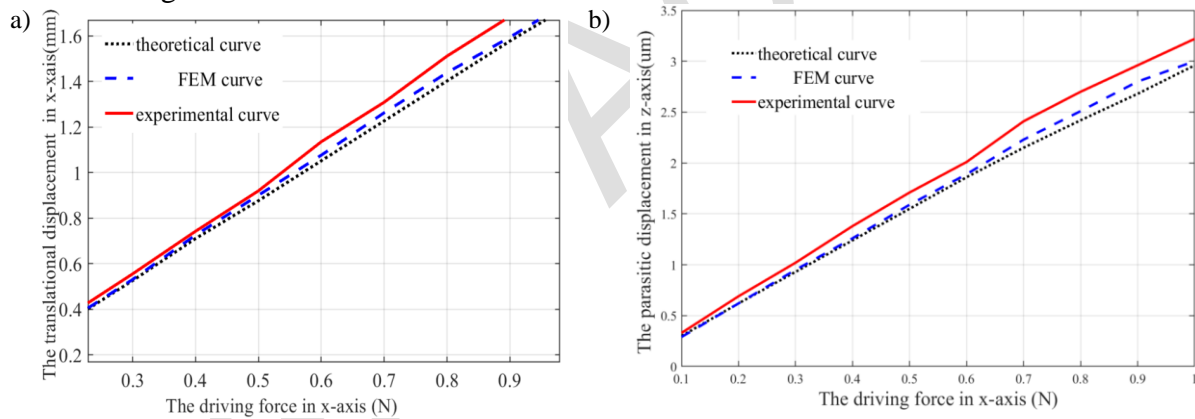


Fig. 6. Analytical and FEA results on 1-DoF CPS

(a) The translational displacement in x -axis, (b) The parasitical displacement in z -axis.

According to hooker's law, the analytical method of determine the theoretical curve of translational displacement is calculated by using the formula as $\Delta x = F_x / K_x$, while the values of input force F_x is increasing on x -axis from 0 ~ 1 N with the step-size as 0.5 N, then the theoretical curve was drawn using the formula above .

In the range of the input driving force, the maximum value of the translational displacement on theoretical calculation and experimental measurement were 1.7527 mm and 1.8013 mm respectively which had a relative error not exceeding 2.8% in the x -axis. And the maximum value of parasitical displacement on theoretical calculation and experimental measurement were 0.0031 mm and 0.0033 mm respectively which had a relative error not exceeding 6.5% in the z -axis. On the other hand, the coupling errors occurring was shown in Fig. 6. over its full travel range in this compliant mechanism. This result verifies the accuracy and effectiveness of the coupling error theoretical model on the 1-DoF CPS.

It could be seen that the error result keeps increasing between the theoretical method and experiment data. The main reason is that this CETM is a simplified error model relatively, the other factors are not considered such as nonlinearity and vibration. But those factors would produce errors to the result of measurement with the increase of the driving force F during the experimental process.

To avoid these problems, some further attempts still need to be done in the future to improve the accuracy of the CETM, such as using lumped compliant unit instead of distributed compliant unit in large deflection compliant mechanism.

4.2. FEA method on 3-DOF CPS

To validate the coupling error theoretical model of the 3-DoF CPS, an FEA model was built in ANSYS Workbench with the FEA model setup as Fig. 7 shown. The material of the compliant guide plates was selected as stainless steel and these performance parameters are detailed in Table 3. Both the translational plates and fixing base have a thickness of 5 mm and the material of them are selected as Aluminium alloy.

The compliant mechanisms were modelled with a size of 1 mm globally and refined in the areas of all the flexure hinges and the compliant plates by element sizes of 0.1 mm as it can be seen in Fig. 7. The shell elements were used to model the flexure hinges and compliant plates. The other physical properties and mesh conditions were selected same as the presented in Section 4.1. The reference coordinate system was consistent with that shown in Fig. 3 and the fixed support constraints were provided on both sides of the end fixing plate. The three axial external driving forces ($F_x = 0.10$ N, $F_y = 0.10$ N, $F_z = 0.10$ N) were applied orthogonally along each coordinate axis at the root of the stylus.

Furthermore, the deformation cloud map results of this 3-DoF compliant guidance mechanism were shown in Fig. 7. The displacements of the compliant translational plates were measured as well as the parasitic displacements which were tracked to evaluate the coupling errors according to Eq.18. The FEA methods were done for all of the investigated compliant mechanisms similarly.

The difference is presented between the theoretical calculations and FEA maximum in Table.4 which shows the parasitic displacements in different coordinates axes as the configurations in the Fig. 7. The relative error of parasitic displacement is 3.75% in z-axial direction. Moreover, the maximum value of coupling error is along the z-axial direction on this configuration of the 3-DoF CPS. Utilizing the (15) and (20) from the aforementioned conclusions, the translational displacements of each axial coordinate could be separated from the 3-DoF integral complaint parallelogram mechanism.

Simultaneously, a minor difference existed between the simulation results and the theoretical calculation values. This discrepancy primarily arises from solely considering the integral deformation of the compliant guidance mechanism, but without individually incorporating the local deformation of the flexible elements in the theoretical analysis. Nevertheless, the local deformation of these flexible elements had an insignificant effect on the motion accuracy of the whole compliant mechanism from a macroscopic viewpoint.

Moreover, the FEA analysis results for the 3-DoF compliant guidance mechanism slightly exceed the theoretical calculation analysis results. The major reason is that the FEA analysis not just account for the deformation of the flexible elements but also includes the deformation of other rigid components. Indeed, the relatively minor elastic deformations are caused by other rigid components under the action of external driving forces.

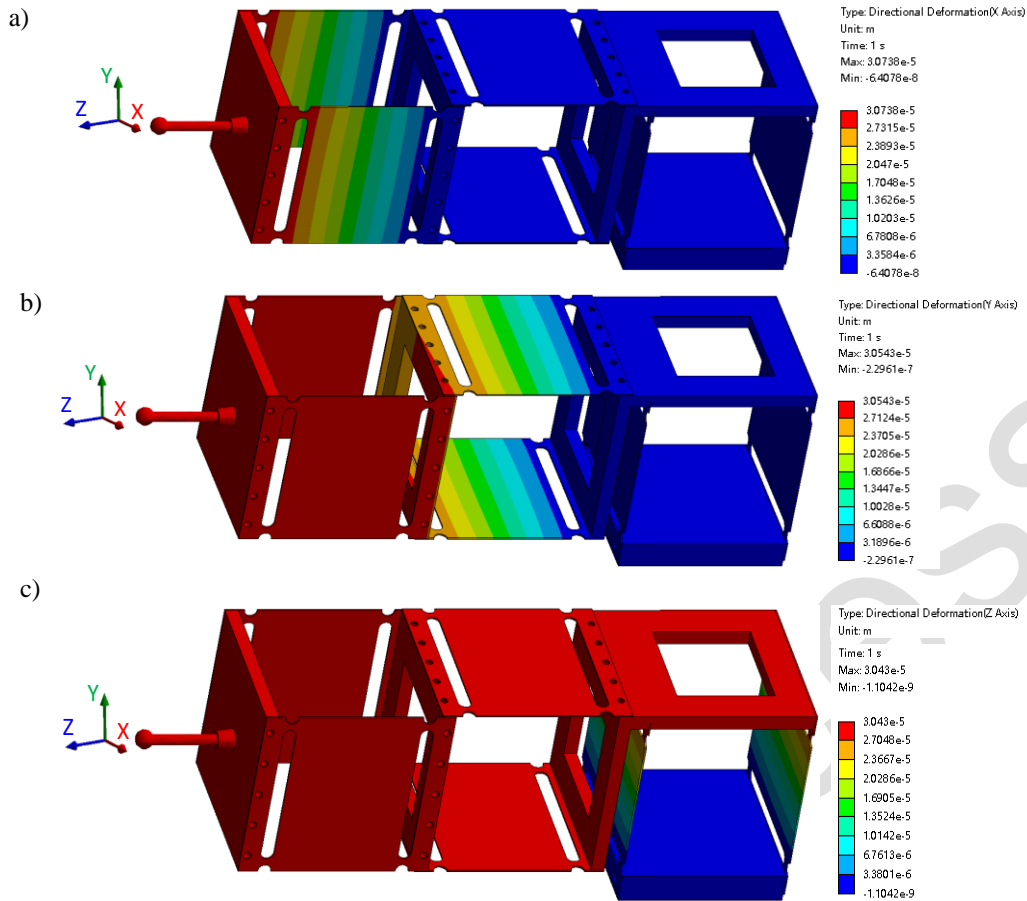


Fig. 7. FEA Model Setup and Results (a) the displacement results in x -axis, (b) the displacement results in y -axis, (c) the displacement results in z -axis.

Furthermore, the research result shows that these measures are effective in mitigating coupling errors, such as reducing input driving force F and the length l of the compliant guide plates, increasing the thickness h of the compliant plates and selecting the flexible materials with relatively high elastic modulus E . Simultaneously, utilizing a reasonable connection configuration can help diminish the negative impact of coupling errors on various coordinate axes.

The main contribution of this work is that the novel CETM is proposed according to the different connection configuration of 3-DoF CPS. This research also provides some feasible and effective approaches for improving the motion accuracy and performances of other multi-dimensional compliant mechanisms.

Table 4. Analytical and FEA maximum displacement results of 3-DoF CPS.

Coordinate direction	Translational displacements(mm)	Theoretical parasitic displacements(μ m)	FEA parasitic displacements(μ m)	Relative error (%)
x -axis	1.7576	2.89	3.07	6.22
y -axis	1.7632	2.91	3.05	4.81
z -axis	1.7689	2.93	3.04	3.7

5. Conclusion

The original contributions of this paper are summarized at the end of Section 1. The main conclusions drawn from this work are as follows:

- (1) Proposing the 3-DoF series CPS based on the 1-DoF compliant mechanisms.
- (2) Applying the pseudo rigid body theory and flexible beam bending theory, the parasitic displacement and coupling error analysis are conducted.
- (3) Establishing the CETM for the 3-DoF CPS and analysing CETM corresponding to the different topological configurations.
- (4) Demonstrating that the configuration of the CETM is independent of the combination order of 3-DoF CPS but related to the coordinate axial vectors of each compliant mechanism.
- (5) Analysing the integral deformation of different configurations on the 3-DoF compliant mechanism through FEA method analysis. The analysis result shows that the relative error of the integral deformation is small. Furthermore, the correctness of the coupling error theory model is well verified by FEA method analysis and experiment investigation.
- (6) The proposed methodology is not only applicable to the 3-DoF CPS but also provides the theoretical foundation for the parasitic displacement and coupling errors of other multi-dimensional compliant mechanisms.

In the subsequent work, the physical prototype and experimental setup will be built on the 3-DoF CPS. Meanwhile, the further investigation would be conducted on the coupling errors of multi-dimensional compliant mechanisms and different topological structures.

Acknowledgments

This work supported by Research Program supported by the National Natural Science Foundation of China under Grant Nos. 51975448.

References

- [1] Howell, L. L., Midha, A., & Norton, T. W. (1996). Evaluation of Equivalent Spring Stiffness for Use in a Pseudo-Rigid-Body Model of Large-Deflection Compliant Mechanisms. *Journal of Mechanical Design*, 118(1), 126–131. <https://doi.org/10.1115/1.2826843>
- [2] Awtar, S., Slocum, A. H., & Sevincer, E. (2006). Characteristics of Beam-Based Flexure Modules. *Journal of Mechanical Design*, 129(6), 625–639. <https://doi.org/10.1115/1.2717231>
- [3] Yin, Z., Huang, Y., Yang, H., Chen, J., Duan, Y., & Chen, W. (2022). Flexible electronics manufacturing technology and equipment. *Science China Technological Sciences*, 65(9), 1940–1956. <https://doi.org/10.1007/s11431-022-2098-1>
- [4] Yuanqiang, L., & Wangyu, L. (2014). Analysis of the displacement of distributed compliant parallel-guiding mechanism considering parasitic rotation and deflection on the guiding plate. *Mechanism and Machine Theory*, 80, 151–165. <https://doi.org/10.1016/j.mechmachtheory.2014.06.005>
- [5] Hao, G., He, X., & Awtar, S. (2019). Design and analytical model of a compact flexure mechanism for translational motion. *Mechanism and Machine Theory*, 142, 103593. <https://doi.org/10.1016/j.mechmachtheory.2019.103593>
- [6] Li, R.-J., Fan, K.-C., Huang, Q.-X., Zhou, H., Gong, E.-M., & Xiang, M. (2016). A long-stroke 3D contact scanning probe for micro/nano coordinate measuring machine. *Precision Engineering*, 43, 220–229. <https://doi.org/10.1016/j.precisioneng.2015.08.001>
- [7] Ling, M., Yuan, L., & Zhang, X. (2024). Geometrically nonlinear analysis of compliant mechanisms using a dynamic beam constraint model (DBCM). *Mechanism and Machine Theory*, 191, 105489. <https://doi.org/10.1016/j.mechmachtheory.2023.105489>
- [8] Malaeké, H., & Moeenfard, H. (2017). A novel flexure beam module with low stiffness loss in compliant mechanisms. *Precision Engineering*, 48, 216–233. <https://doi.org/10.1016/j.precisioneng.2016.12.004>

- [9] Awtar, S., & Mariappan, D. D. (2017). Experimental measurement of the bearing characteristics of straight-line flexure mechanisms. *Precision Engineering*, 49, 1–14. <https://doi.org/10.1016/j.precisioneng.2016.12.014>
- [10] Shi, H., Yang, G., Li, H. N., Zhao, J., Yu, H., & Zhang, C. (2024). A flexure-based and motion-decoupled XYZ nano-positioning stage with a quasi-symmetric structure. *Precision Engineering*, 89, 239–251. <https://doi.org/10.1016/j.precisioneng.2024.06.014>
- [11] Zhang, C., Yu, H., Yang, M., Chen, S., & Yang, G. (2022). Nonlinear kinetostatic modeling and analysis of a large range 3-PPR planar compliant parallel mechanism. *Precision Engineering*, 74, 264–277. <https://doi.org/10.1016/j.precisioneng.2021.09.019>
- [12] Hao, G., & Yu, J. (2016). Design, modelling and analysis of a completely-decoupled XY compliant parallel manipulator. *Mechanism and Machine Theory*, 102, 179–195. <https://doi.org/10.1016/j.mechmachtheory.2016.04.006>
- [13] Ni, Z., Zhang, D., Wu, Y., Tian, Y., & Hu, M. (2010). Analysis of parasitic motion in parallelogram compliant mechanism. *Precision Engineering*, 34(1), 133–138. <https://doi.org/10.1016/j.precisioneng.2009.05.001>
- [14] Li, J., Cai, J., Wen, J., Zhang, Y., & Wan, N. (2020). A parasitic type piezoelectric actuator with the asymmetrical trapezoid flexure mechanism. *Sensors and Actuators A: Physical*, 309, 111907. <https://doi.org/10.1016/j.sna.2020.111907>
- [15] Wu, H., Lai, L., Zhang, L., & Zhu, L. (2022). A novel compliant XY micro-positioning stage using bridge-type displacement amplifier embedded with Scott-Russell mechanism. *Precision Engineering*, 73, 284–295. <https://doi.org/10.1016/j.precisioneng.2021.09.014>
- [16] Wu, K., Zheng, G., & Hao, G. (2021). Efficient spatial compliance analysis of general initially curved beams for mechanism synthesis and optimization. *Mechanism and Machine Theory*, 162, 104343. <https://doi.org/10.1016/j.mechmachtheory.2021.104343>
- [17] Cui, L., & Awtar, S. (2019). Experimental validation of complex non-minimum phase zeros in a flexure mechanism. *Precision Engineering*, 60, 167–177. <https://doi.org/10.1016/j.precisioneng.2019.08.002>
- [18] Arredondo-Soto, M., Cuan-Urquizo, E., & Gómez-Espinosa, A. (2022). The compliance matrix method for the kinetostatic analysis of flexure-based compliant parallel mechanisms: Conventions and general force–displacement cases. *Mechanism and Machine Theory*, 168, 104583. <https://doi.org/10.1016/j.mechmachtheory.2021.104583>
- [19] Meli, F., Kueng, A., & Thalmann, R. (2005). Ultra precision micro-CMM using a low force 3D touch probe. In J. E. Decker & G.-S. Peng (Eds.), *SPIE Proceedings* (Vol. 5879, p. 58790S). SPIE. <https://doi.org/10.1117/12.618692>
- [20] Gallardo, A. G., & Pucheta, M. A. (2024). Synthesis of parallel flexure stages with decoupled actuators using sum, intersection, and difference of screw systems. *Mechanism and Machine Theory*, 192, 105526. <https://doi.org/10.1016/j.mechmachtheory.2023.105526>
- [21] Ling, M., Howell, L. L., Cao, J., & Chen, G. (2020). Kinetostatic and Dynamic Modeling of Flexure-Based Compliant Mechanisms: A Survey. *Applied Mechanics Reviews*, 72(3). <https://doi.org/10.1115/1.4045679>
- [22] Xu, H., Zhang, X., Wang, R., Zhang, H., & Liang, J. (2023). Design of an SMA-driven compliant constant-force gripper based on a modified chained pseudo-rigid-body model. *Mechanism and Machine Theory*, 187, 105371. <https://doi.org/10.1016/j.mechmachtheory.2023.105371>
- [23] Mattson, C. A., Howell, L. L., & Magleby, S. P. (2004). Development of Commercially Viable Compliant Mechanisms Using the Pseudo-Rigid-Body Model: Case Studies of Parallel Mechanisms. *Journal of Intelligent Material Systems and Structures*, 15(3), 195–202. <https://doi.org/10.1177/1045389x04033256>
- [24] Sorgonà, O., Serafino, S., Giannini, O., & Verotti, M. (2024). Analysis of compliant mechanisms with series and parallel substructures through the ellipse of elasticity theory. *International Journal of Solids and Structures*, 298, 112847. <https://doi.org/10.1016/j.ijsolstr.2024.112847>
- [25] Bai, R., Chen, G., & Awtar, S. (2021). Closed-form solution for nonlinear spatial deflections of strip flexures of large aspect ratio considering second order load-stiffening. *Mechanism and Machine Theory*, 161, 104324. <https://doi.org/10.1016/j.mechmachtheory.2021.104324>
- [26] Wang, F., Zhao, X., Huo, Z., Shi, B., Liang, C., Tian, Y., & Zhang, D. (2021). A 2-DOF nano-positioning scanner with novel compound decoupling-guiding mechanism. *Mechanism and Machine Theory*, 155, 104066. <https://doi.org/10.1016/j.mechmachtheory.2020.104066>

- [27] Li, C., & Chen, S.-C. (2023). Design of compliant mechanisms based on compliant building elements. Part I: Principles. *Precision Engineering*, 81, 207–220. <https://doi.org/10.1016/j.precisioneng.2023.01.006>
- [28] Ochoa, O., Betancourt-Tovar, M., Espinosa-Curiel, A. S., Castro-Avilés, A., Granados, N., & Cuan-Urquizo, E. (2024). Novel compliant mechanism-based auxetic metamaterial: Kinematic and experimental analysis. *International Journal of Mechanical Sciences*, 279, 109478. <https://doi.org/10.1016/j.ijmecsci.2024.109478>



Huaibo Qiang received the Master Engineering degree from the Xi'an Technological University, China, in 2007. As a lecturer, he has been engaged in teaching and research work on mechanical and electrical engineering over twenty years. His research focuses on precision measurement theory and instrument design, compliant mechanism design theory and application. He is currently

pursuing the Ph.D. degree on Mechanical and Electronic Engineering.



Qiang Huang received the Master Engineering degree from the Xi'an Technological University, China, in 2007. He is currently a senior engineer at the Northwest Institute of Mechanical and Electrical Engineering. His research activities focus on the analysis of complex structural forces and the integration of electromechanical systems.



Hongxi Wang received the Ph.D. degree from Xidian University, China, in 2006. He is currently a Full Professor and the Dean of School of Mechatronic Engineering in the Xi'an Technological University. His research activity focuses on precision measurement theory and instrument design, compliant mechanisms and intelligent sensors.

Early Access